Microphysical Characteristics through the Melting Region of a Midlatitude Winter Storm

GRACIELA B. RAGA, RONALD E. STEWART AND NORMAN R. DONALDSON

Cloud Physics Research Division, Atmospheric Environment Service, Downsview, Ontario Canada

(Manuscript received 13 May 1990, in final form 18 September 1990)

ABSTRACT

The microphysical characteristics of a precipitation type transition region within a midlatitude winter storm are discussed in relation to the background thermodynamic and kinematic fields. A deep region in which the temperature was close to 0°C (the transition region) was observed along the Atlantic coastline of Nova Scotia. This transition region was approximately 30 km wide and about 2 km deep. At 80 kPa, a large horizontal temperature gradient marked the boundary between the transition region and the colder air. The observed thermal structure is linked to diabatic processes, and in particular, to the freezing of small droplets, the refreezing of semi-melted particles and the melting of precipitation. Large, partially melted aggregates were located just downwind of the deep transition region. Particle trajectories near the transition region are very sensitive to the background temperature and wind fields and may lead to regions of reduced and enhanced concentrations at the surface and aloft. A conceptual model of the flow fields suggests that this case resembles warm and cold conveyor belts similar to those found in synoptic systems, but on a smaller scale. The transition region in this case is located at the boundary between the warm and cold conveyor belts.

1. Introduction

Extratropical cyclones account for most of the precipitation observed in midlatitudes during the winter months. This precipitation, which can be in the form of rain, snow, freezing rain, or ice pellets is the result of processes acting at different scales: from the synoptic down to the microphysical. The localized precipitation from these synoptic systems can lead to problems such as flooding, accretion of ice onto structures at the surface and major snow accumulations.

The mesoscale structure and the precipitation patterns within midlatitude winter storms have been the object of numerous studies in the past (see Hobbs 1978, for a review). In particular, the nature of the mesoscale bands embedded in synoptic systems has been thoroughly investigated, leading to explanations often based on the concept of symmetric instability (Parsons and Hobbs 1983; Sanders and Bosart 1985; Knight and Hobbs 1988; among others).

Relatively little work has focused on the regions within the storms in which several types of precipitation occur in close proximity. Stewart and King (1987a,b) used radar to investigate the mesoscale characteristics of storms during freezing rain events and noted that observations at the boundary between rain and snow were consistent with a mesoscale circulation driven by melting snow (Lin and Stewart 1986). Using surface and rawinsonde data Stewart and Patenaude (1988) examined 14 rain–snow boundaries and freezing rain episodes and found them to be closely coupled features.

The small scale characteristics and the distribution of the hydrometeors within the region of a storm in which a transition between precipitation types occur (hereafter called the transition region) still remain to be investigated. A simultaneous study of the hydrometeors in association with the thermodynamic and kinematic fields is necessary to understand the nature and distribution of precipitation at the surface.

The purpose of this article is to use aircraft data to document the microphysical features of a transition region and to relate them to the background thermodynamic and kinematic fields. The case chosen for examination was 22 February 1986, sampled during the Canadian Atlantic Storms Program (CASP) field project (Stewart et al. 1987).

The organization of this paper is as follows: section 2 provides background on the case study; section 3 presents the high resolution thermodynamic and kinematic fields derived from aircraft data. The microphysical fields are discussed in section 4. In section 5 we estimate trajectories of hydrometeors through the observed temperature and wind fields. Further discussion and conclusions are presented in section 6.

2. Background

A storm formed over the Gulf of Maine on 22 February 1986 and moved, without deepening, south of Nova Scotia. During the period of this study, the low pressure center (the minimum pressure observed was

Corresponding author address: Dr. Graciela B. Raga, Atmospheric Research Service (ARMP), 4905 Dufferin St., Downsview, Ontario M3H 5T4, Canada.

99.4 kPa) was analyzed to be 200 km south of the coastline and moved roughly 50 km towards the east. At 80 kPa, a closed contour in the height field was analyzed to the WSW of the region sampled, but above 80 kPa no closed contours were analyzed. A synoptic discussion of this case has been presented by Stewart et al. (1990). This storm produced a large amount of precipitation over its lifetime as well as a variety of precipitation types at the surface. The heaviest precipitation was concentrated along the southern Nova Scotia coastline and it fell as a mixture of snow, freezing rain, ice pellets and rain.

A DC-3 instrumented aircraft flew through the storm for nearly 4 h, measuring standard thermodynamic parameters, horizontal winds and cloud and precipitation particles (Stewart et al. 1987). The flight track is shown in Fig. 1. The aircraft flew three constant pressure segments along the 63°W meridian at: 86.5 (1358–1405 UTC), 80 (1420–1448 UTC) and 71 kPa (1505–1520 UTC). This paper will focus on this cross section although information from other flight legs is used to supplement the study.

3. Thermodynamic and kinematic fields

Stewart et al. (1990) show the thermodynamic and kinematic fields along the cross section at 63°W utilizing aircraft data averaged over five minute periods. In this study we have used high resolution aircraft data (1 Hz) and reanalyzed the fields. The temperature field is shown in Fig. 2, where we have included information from surface stations as well as from the 1144 UTC rawinsonde at Summerside (Prince Edward Is.) and the 1327 UTC rawinsonde at Shearwater (Nova Scotia).

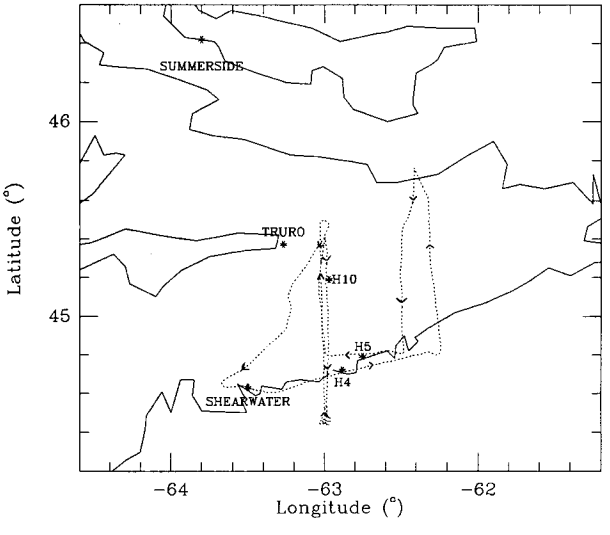

FIG. 1. Flight tracks of the DC-3 (dotted line) aircraft as it flew through the storm between 1220 and 1600 UTC 22 February 1986. The solid line denotes the coastline and H4, H5, and H10 represent automated surface stations.

There are several remarkable features in this cross section:

(i) The deep region (from the surface to 78 kPa) in which the temperature ranges between −0.5° and +0.5°C. This region is deepest near the coastline and has a horizontal extent of ≈30 km.

(ii) The large temperature gradient (2.5°C over approximately 4 km) at the northern edge of the transition region at 80 kPa.

(iii) The very weak horizontal temperature gradient immediately to the north of the transition region for about 70 km.

(iv) The localized packing of the isotherms at 80 kPa, extending less than 10 kPa in the vertical.

Figure 3 shows the field of equivalent potential temperature, θ_e, for the same cross section. The region of 0°C at 80 kPa (Fig. 2) appears as a localized maximum in θ_e, and the tight horizontal gradient at the north edge is very likely linked to the diabatic effects of phase transitions, in particular, the freezing of water droplets that collide with ice crystals present. We have estimated maximum vertical velocities of the order of 40 cm s^{-1} from the θ_e field at 86.5 kPa. This value, derived under the assumption of a 2-D stationary flow, probably represents an overestimate of the true upward motions.

The horizontal wind fields are shown in Fig. 4. There is convergence in the north–south wind component, v, at 86.5 kPa and there is divergence at 80 kPa (Fig. 4b). At 71 kPa the wind varies little along the flight track, and it has a southerly component of about 10 m s^{-1}. This distribution of the v-component is consistent with localized convergence at lower levels forcing air upwards as it progresses northward. Furthermore, we have calculated the mass streamfunction and we find that it indicates upward and northward motion consistent with the θ_e cross section (Fig. 3). The contours of the east–west component, u, (Fig. 4a) indicate that there is an easterly jet (with a maximum value of 18 m s^{-1}) centered at 86.5 kPa; values of this component drop sharply to zero at the southern edge of this flight leg. The observations at 80 kPa indicate weak westerlies (approximately 4 m s^{-1}), which increase with height above that level. The transition to easterlies at 80 kPa occurs half way through the flight leg.

4. Cloud and precipitation characteristics

a. Overview

Figure 5 shows the transition region from the temperature field with averaged cloud and precipitation information superimposed at selected locations. The wide variation in the microphysical parameters over the region of interest is clearly evident. The number concentration of cloud droplets measured by the Forward Scattering Spectrometer Probe (FSSP) varies from values close to 10 cm^{-3} in the region of below freezing temperatures to more than 100 cm^{-3} in the 0°C region

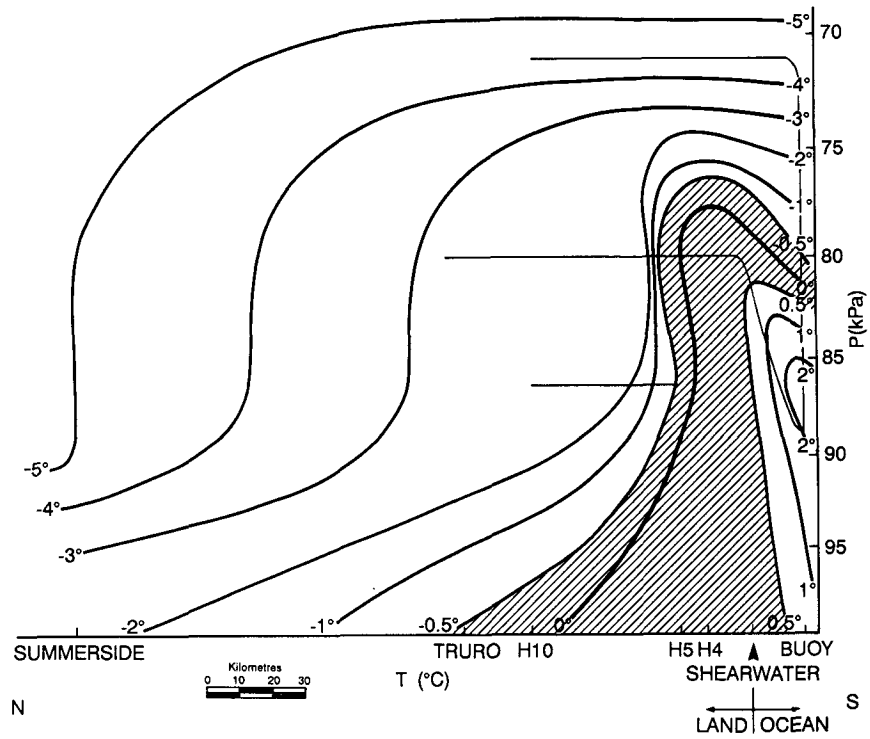

FIG. 2. North–south vertical cross section along the 63°W meridian showing the transition region (shaded, see text), the DC-3 flight tracks (light solid lines) and the temperature field in °C.

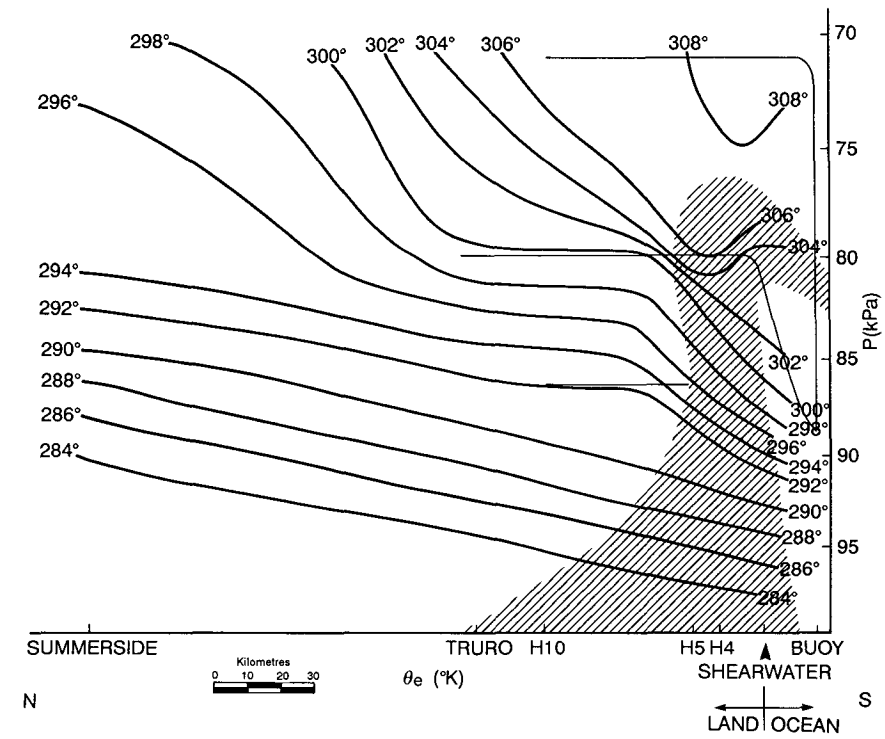

FIG. 3. As in Fig. 2 but for the equivalent potential temperature, θ_e, in °K.

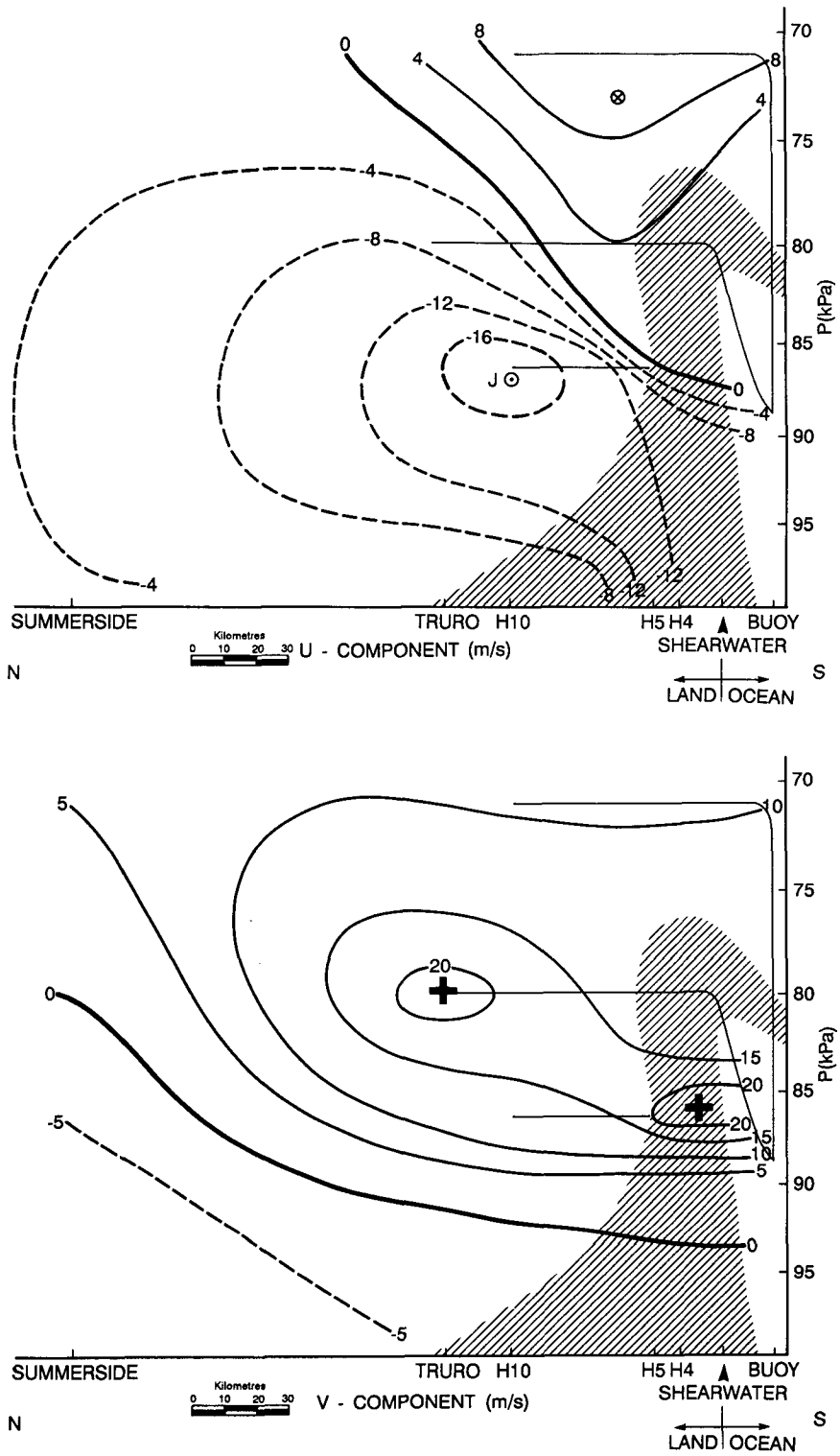

FIG. 4. As in Fig. 2 but for (a) the u and (b) v components of the wind, in m s^{-1}. Winds from the south and west are defined positive.

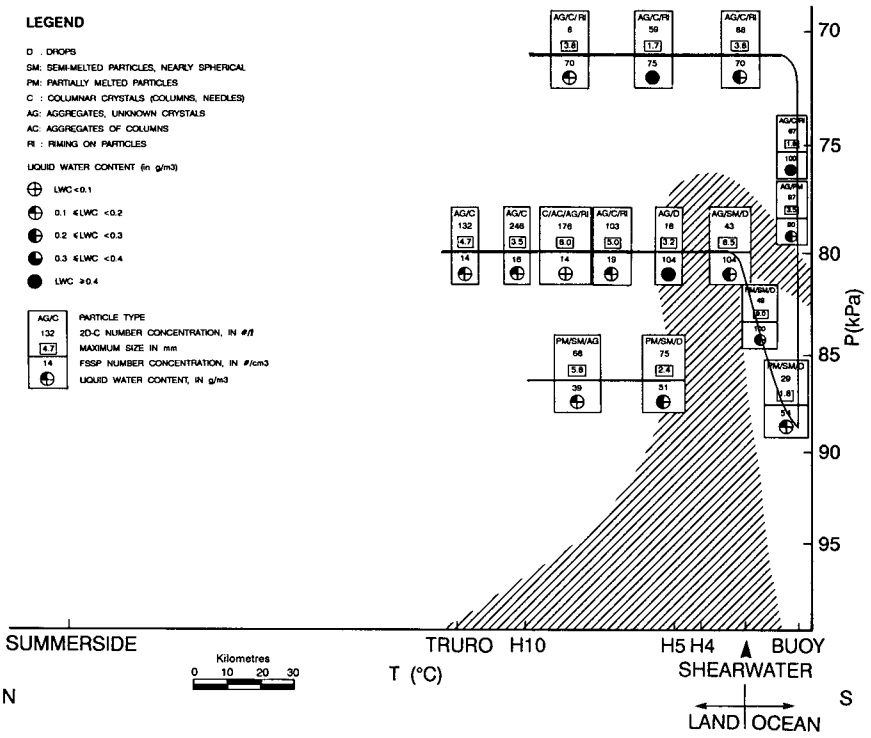

FIG. 5. As in Fig. 2 but with cloud and precipitation information at selected locations. The values shown at constant pressure are 5 min averages, while the values during descent and ascent are 1 min averages.

at 80 kPa. Values around 70 cm^{-3} (5 min averages) are observed at 71 kPa. The cloud spectra (in the range between 0 and 35 μm measured by the FSSP) also show a large variability and will be discussed more thoroughly later in this section.

The cloud liquid water contents were derived from the FSSP cloud spectra. The sensing element in the King probe burnt out five minutes after take-off and the Johnson–Williams device was mounted too close to the pilon and was therefore very sensitive to the yaw angle. The FSSP liquid water contents admmitedly represent an underestimate of the true liquid water contents when large droplets are present, but no independent measurements are available for this case study. At 80 and 86.5 kPa the highest water contents were observed in the transition region, which at 86.5 kPa is adjacent to the region of large horizontal wind shear (see Fig. 4a). These peaks in water content are associated with the ascent of relatively warm and moist air from the south. At 71 kPa there was another peak in liquid water content (1 s measurements of up to 0.6 g m^{-3}) located above the transition region. The upwind horizontal flow fields and high water contents at 75 kPa suggest that the peak at 71 kPa is not linked to the peaks within the transition region. The Shearwater rawinsonde indicated that the air was potentially unstable above 75 kPa, and some embedded convection could possibly be responsible for the high water contents observed at that level.

A 2D cloud particle imaging probe (25–800 μm) was used to measure the precipitation spectra. The center-in technique (Heymsfield and Parrish 1979) was used to calculate the total number concentration of droplets; when ice particles were present, the extended area technique (Gordon and Marwitz 1984) was utilized. The concentrations were integrated over periods of 1 and 5 min. The largest concentrations were observed downwind of the transition region at 80 kPa, where the FSSP droplet concentrations were smallest. The particles consisted mostly of aggregates of columns, with some evidence of riming; the temperature was approximately −2.8°C. Maximum sizes ranged from 3.5 to 8.0 mm.

At 71 kPa, the 2D particle images illustrated that there were a large number of needles and columns as well as some aggregates up to 3.8 mm in size. The temperature at this level ranged between −4° and −5°C. Rimed particles were frequently observed at this level where the liquid water content was high. The presence of substantial numbers of columnar crystals and the high concentrations of ice particles in general imply that ice multiplication was occurring. It is possible that both collisions between crystals (Vardiman 1978) and riming processes (Hallett and Mossop 1974)

contributed to an enhancement of particle concentrations.

In the flight leg at 86.5 kPa ($T = -2.5°C$) the ice particles were considerably different from those observed at 80 and 71 kPa. Although the maximum sizes were comparable, the images at 86.5 kPa showed that the particles were partially melted (some rounded edges in aggregates of columns), suggesting that these particles had crossed the transition region.

b. Observations through 0°C

As seen in Fig. 2, the transition region extended vertically from the surface to approximately 78 kPa. The DC-3 aircraft made two horizontal passes through this region and an ascent through the nearly horizontal 0°C isotherm to the south. Studies in the past (Stewart et al. 1984; Willis and Heymsfield 1989) have reported aircraft observations through horizontal 0°C isotherms, linked to layers of enhanced radar reflectivities. We are not aware of any previously reported information on the microphysical characteristics through vertical 0°C isotherms.

1) VERTICAL PASS

The DC-3 made a spiral ascent from 90 to 71 kPa (1453–1505 UTC) and crossed through a shallow (180 m) transition layer ($|T| \leq 0.5°C$) centered at 82 kPa (1.7 km). A thorough comparison between our observations and those presented by Stewart et al. (1984) and Willis and Heymsfield (1989) is not possible because we lack information on large particles (in the 2D–P range). Moreover, our observations did not show an isothermal layer at 0°C, suggesting that microphysical processes were not important in the formation of the shallow transition layer observed. We briefly summarize our microphysical observations through the transition layer as follows.

The concentration of 2D–C particles increased with height through the transition layer from 30 to 50 L^{-1}, while the concentration of particles with sizes larger than 500 μm increased from 0.8 to 70 L^{-1}. In contrast, the concentration of cloud droplets (measured by an FSSP) remained virtually unchanged through the melting layer, at around 80 cm^{-3}. The liquid water content was higher than 0.1 g m^{-3} throughout the ascent, with a peak value of 0.5 g m^{-3} at 2.2 km.

At temperatures below 0°C many of the particles (measured by the 2D–C probe) were rimed aggregates, while others may have been rimed ice crystal fragments. Close to 0°C, a large number of the particles appeared to be partially melted. The presence of the cloud liquid water may have affected the onset of melting, since accretion of water onto crystals at temperatures below 0°C could raise their temperature by about 0.3°–0.5°C (for liquid water contents around 0.3 g m^{-3}). The warmest temperature at which a partially melted particle was observed was 1°C. Although ice may have been present within particles at warmer temperatures, all these particles were circular in appearance with maximum diameters of about 1.5 mm. The largest observed particles occurred close to the top of the transition layer and were about 3.5 mm in size. Due to the limited sample size of the probes, it is probable that larger particles were present but undetected.

2) HORIZONTAL PASS

In this section we concentrate on the microphysical characteristics encountered on the flight segments crossing horizontally through the transition region, at 80 and 86.5 kPa.

Figure 6 shows the variation of several thermodynamic and microphysical parameters at 80 kPa in the region with temperatures ranging from −3° to 0.5°C (1425–1445 UTC). The ordinate is given by the distance Δy from a reference location y_o, which corresponds to the north edge of the transition region. The main rise in temperature (Fig. 6a) occurred over less than 1 min, which corresponds roughly to about 4 km. There was a broad region about 30 km across in which the temperatures were close to 0°C. Associated with this background temperature field, there was a dramatic increase in the liquid water content (Fig. 6b) and the FSSP number concentration (Fig. 6c). Values of these parameters were much lower in the colder air than within the transition region, in which liquid water contents exceeded 0.3 g m^{-3} and droplet concentrations exceeded 200 cm^{-3}. The 2D–C concentrations (Fig. 6d) also exhibited a correlation to the background temperature field. Although values within the transition region and more than 10 km away from it were similar, there was a dramatic fall-off in concentration immediately adjacent to the transition region. The concentration of particles with sizes larger than 500 μm was virtually zero within the transition region; only particles with sizes smaller than 500 μm were present, in concentrations of around 30 L^{-1}. In the region sampled between $\Delta y = 4$ km and $\Delta y = 64$ km, the temperature ranged between −2.5° and −3°C and the cloud droplet size distribution was characterized by low number concentrations, mean radii of about 8 μm, and standard deviation of the radius of about 5 μm. As soon as 0°C was reached, the number concentrations increased dramatically (at least by a factor of two and up to one order of magnitude); at the same time the mean radius and the standard deviation dropped substantially.

The fine-scale variation of the FSSP spectra across the edge of the transition is illustrated in Fig. 7. Note the significant differences in the number concentrations and mean radii between spectra colder than 0°C and those in the transition region. The total number concentration increased an order of magnitude from 13 to 148 cm^{-3} over about 3 km, and this was correlated with an increase in temperature from −2° to 0°C. The

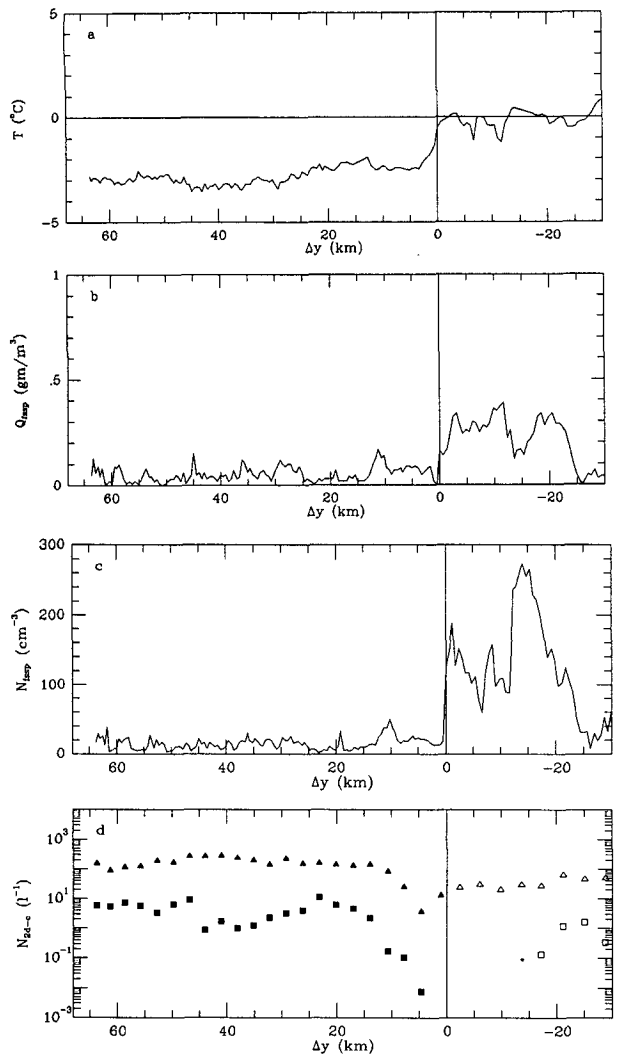

FIG. 6. Several parameters as a function of the distance Δy from the edge of the transition region for the flight leg at 80 kPa. The vertical line at $\Delta y = 0$ denotes the edge of the transition region; $\Delta y < 0$ corresponds to $T > -0.5$°C, and $\Delta y > 0$ corresponds to $T < -0.5$°C. (a) Temperature, T; (b) liquid water content, Q_{FSSP}; (c) FSSP number concentration, N_{FSSP}; and (d) total number concentration of particles measured by 2D–C, N_{2Dc}, integrated over 1 min. The triangles correspond to concentrations of particles with sizes larger than 100 μm and the squares to concentrations of particles with sizes larger than 500 μm. Filled-in symbols represent ice particle concentrations.

spectrum observed at 1441:40 UTC has a total number concentration of 189 cm^{-3}, with about 70% of the droplets less than 7.4 μm in diameter.

Figure 8 illustrates some of the characteristics of the 2D images as a function of temperature and the distance Δy. At 80 kPa and −3°C (45 km north of y_o) a considerable number of small ice particles (mostly of indistinguishable habit, with some columns and needles) were found, as well as a few large aggregates (up to 4 mm in size). At −2.5°C and 25 km north of y_o we also observed small particles (mostly columns, needles and some of undistinguishable habit) and aggregates up to 8 mm in size. At 6 km from y_o and still at −2.5°C there was a virtual void of particles larger than 25 μm; very few aggregates were observed in this region. At temperatures between −2° and 0.5°C no large particles were present.

The 2D size distributions at 80 kPa shown in Fig. 9 were observed before, during and after the temperature rise from −2.5° to 0°C. Figure 9a illustrates the spectrum observed about 20 km north of the edge of the transition region (1434 to 1438 UTC), while the temperature was close to −2.5°C. Particles up to 3.9 mm in size were observed with concentrations above the threshold. The region with temperatures ranging from −2.5° to −1.7°C had virtually no particles larger than 25 μm in size. The spectrum observed through the transition region (Fig. 9b) differs from the one shown in Fig. 9a in that the number concentrations were about an order of magnitude lower and the largest particles with concentrations above the threshold were now only 375 μm in size. A similar distribution was observed several kilometers inside the transition region (Fig. 9c).

A second horizontal pass through the transition region was made at 86.5 kPa. In this instance, the aircraft flew from within the transition region towards colder temperatures. As in the 80 kPa pass, there was a sharp gradient in the horizontal temperature field as temperatures changed from near 0°C to below this value. At this level the 2D images (Fig. 10) between −0.4° and −2°C show a substantial difference from the images obtained at similar temperatures at 80 kPa. At −2° and −3°C there is evidence of melting and re-

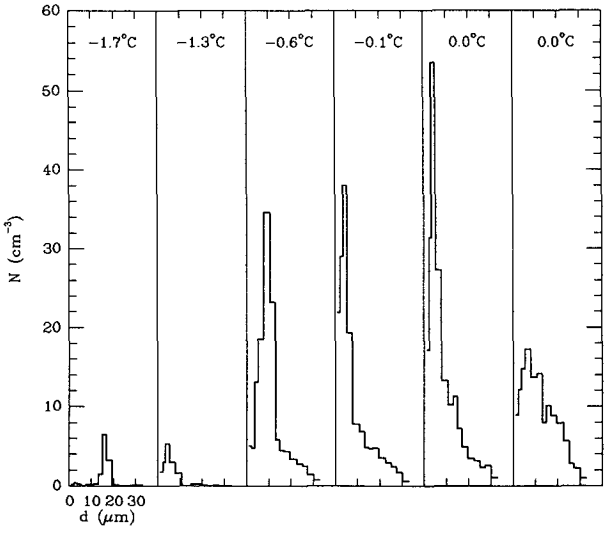

FIG. 7. Droplet size distributions measured by an FSSP every 10 s (~650 m apart) through the sharp horizontal temperature gradient at 80 kPa.

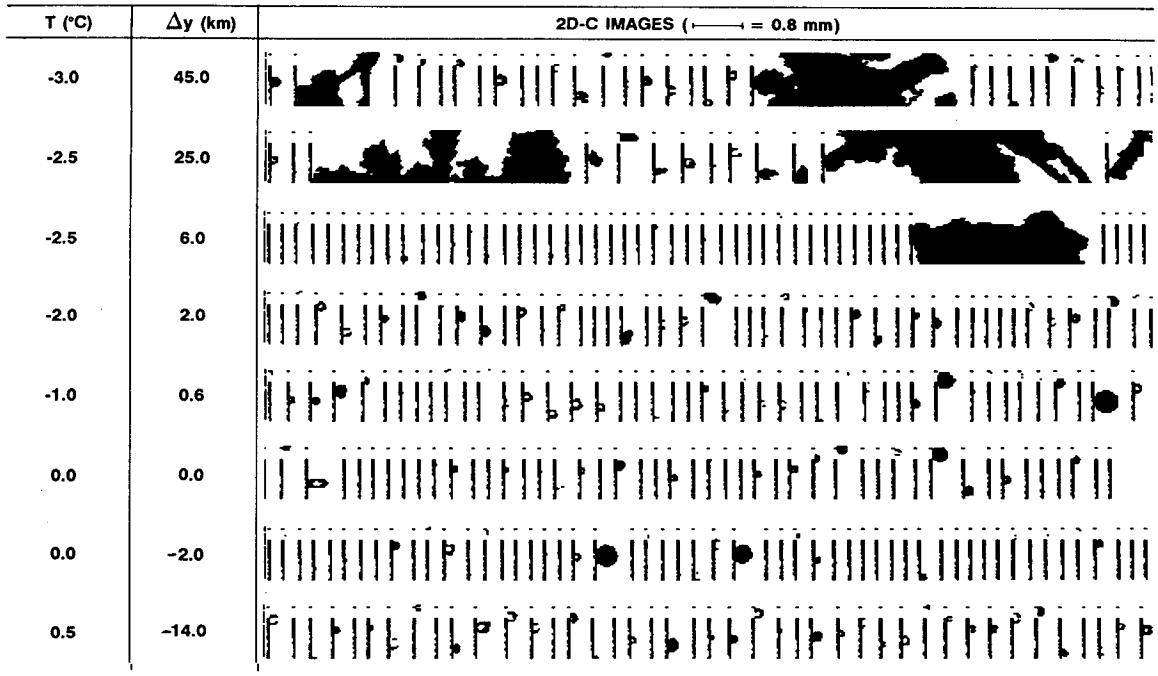

FIG. 8. Two-dimensional images as a function of the air temperature and the distance Δy from the edge of the transition region at 80 kPa.

freezing, suggesting that particle trajectories crossed the 0°C isotherm somewhere above this level.

5. Particle trajectories

In this section we investigate the influence of the observed temperature field (see Fig. 2) on the distribution of hydrometeors and the organization of precipitation. We have calculated particle trajectories in a two-dimensional domain of 150 km in the horizontal and 3 km in the vertical. The observed wind (N–S component) and temperature fields were gridded with a resolution of 7.5 km in the horizontal and 100 m in the vertical. Estimated vertical motions, with a maximum value of 40 cm s^{-1} (see section 3) downwind of the transition region, were also included. The basic calculations assume that the atmosphere is saturated with respect to liquid water but no cloud water is present.

The microphysical model used in the calculations is described by Donaldson and Stewart (1990). The model accounts for particle growth by deposition and accretion, it allows for both melting and freezing, but it does not account for aggregation. Particles of different sizes (assumed to be spherical) are introduced near the top of the domain and are followed as they fall through the observed temperature and wind fields. The choice of appropriate values for the density (ie diameter) of the assumed spherical ice crystal particles is not clear-cut. The diameter of a particle affects the calculation of the terminal velocity and of the heat and vapor fluxes from the particle. We might think of the diameter as being a "diameter of influence", within which the momentum, vapor and temperature are those of the particle surface. Low values of the particle density result in improved terminal velocities at the expense of larger fluxes from the increased surface area. In this study we focus on the timing and location of particles at the ground and, therefore, we have chosen particle densities to best match terminal velocities. As a particle melts, its terminal velocity smoothly changes to that of a raindrop as determined from the parameterization of Best (1950). The initial particles are light snowflakes of density 5 kg m^{-3} (Matsuo and Sasyo 1981) and their terminal velocities are 0.3, 0.9, and 1.4 m s^{-1} for masses equivalent to 0.5, 1.5, and 3.0 mm diameter drops, respectively.

The computed trajectories of particles having a mass equivalent to a 1.5 mm drop are shown in Fig. 11. The results indicate that there is an enhanced separation of particles in the vicinity of the transition region. Particles which near the top of the domain are located only 5 km apart, reach the surface up to 20 km apart. In the region with temperatures above 0°C, the particles melt, achieve a high terminal velocity, and rapidly descend to the ground. In contrast, particles which do not melt never achieve high terminal velocities and, therefore, are carried much further downwind. Neither the elimination of vertical air motions nor the elimination of depositional growth onto the snow particles alters the basic trajectory pattern.

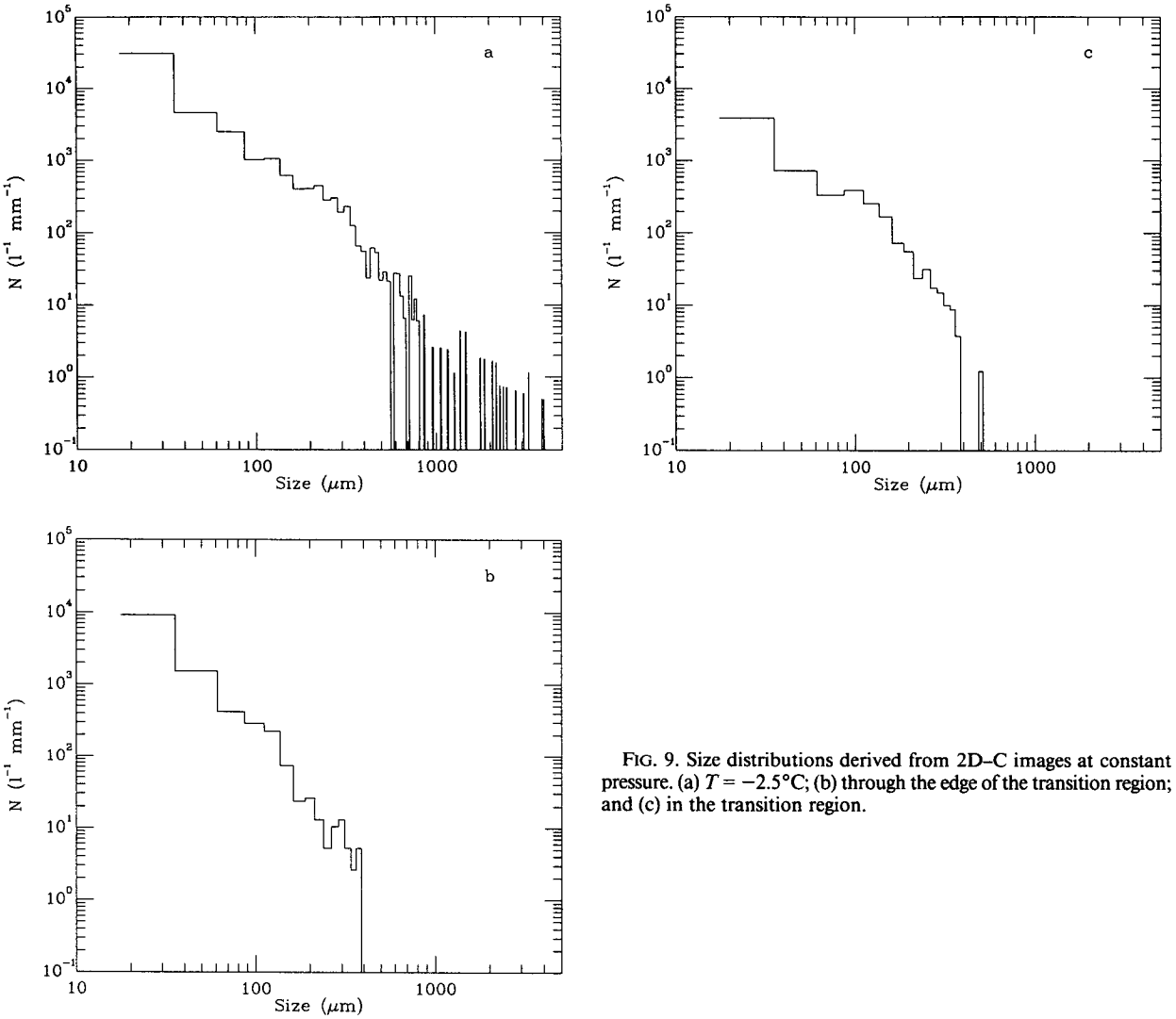

FIG. 9. Size distributions derived from 2D–C images at constant pressure. (a) $T = -2.5$°C; (b) through the edge of the transition region; and (c) in the transition region.

Figure 12 shows the variation of particle characteristics for some of the 1.5 mm equivalent diameter particles. The temperature of particle *A* (Fig. 12a) rose to 0°C after descending about 700 m and then required only 140 s (150 m) to melt in the region with air temperatures up to 1.2°C. The particle which passed through the "nose" of the transition region (particle *B*, Fig. 12b) also began to melt but its temperature reached only 0.01°C. Approximately 2% of the mass melted before the particle refroze in the colder air. Particles which were always at temperatures below 0°C (particle *C*, Fig. 12c) experienced the highest supersaturation and, thus, grew quickly by condensation.

The calculated trajectories for selected 0.5, 1.5, and 3.0 mm equivalent diameter drops are shown in Fig. 13. When we introduce particles of different sizes at a single location, we observe that the largest one always reaches the surface upwind (south) of the others. This effect is least pronounced in the rain region and most pronounced in the transition region. In particular, particles of different sizes originating at location *D* reach the surface up to 40 km apart. The two largest particles fall more vertically, entering the warm air and melting. In contrast, the smallest particle is carried so far downwind, through the transition region and again through cold air, that it does not melt.

To test the effect of particle density on the pattern of particle positions at the ground, the trajectories of denser (37 kg m^{-3}) ice crystal particles were also examined. With their increased fall velocity, these particles were less influenced by the background velocity field and fell more vertically, but the overall trajectory pattern seen in Fig. 11 was maintained. The gap between landing locations of particles (1.5 mm initial equivalent diameter) which melted and those which did not was therefore lessened to about 8 km, for par-

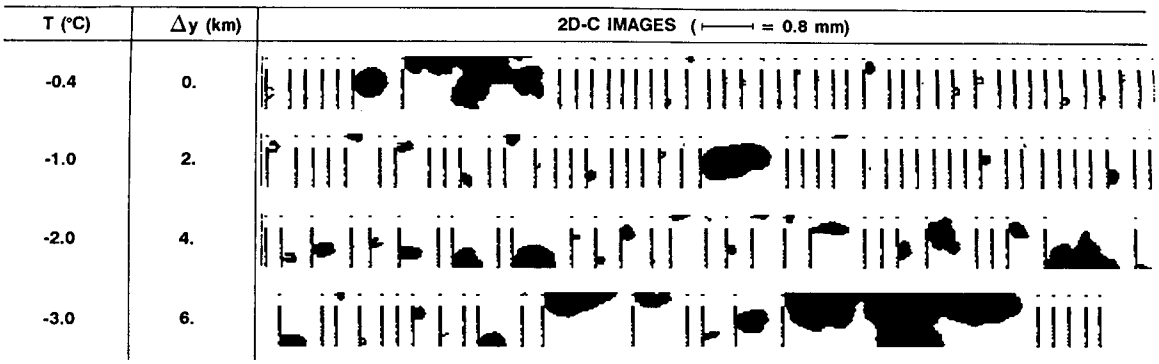

FIG. 10. As in Fig. 8 but for the flight leg at 86.5 kPa.

ticles starting 5 km apart, and its location moved toward the warm air. Similarly, in simulations which included accretion of cloud water onto the particles the increased terminal velocities of the growing particles resulted in more vertical paths and a lessened gap at the ground.

The calculated trajectories of particles of different sizes imply that there may be a reduction of particle concentrations in a zone close to the transition region and an enhancement at colder temperatures.

6. Discussion

We have presented observations obtained in a midlatitude winter storm centered just off the coast of Nova Scotia. The region of the storm sampled by the aircraft was about 200 km northeast of the analyzed low pressure center at the surface. We now discuss the main characteristics observed and synthesize them into a conceptual model.

a. The transition region

A transition region (where the temperature ranged between −0.5° and +0.5°C) extended from the surface to 78 kPa and was about 30 km wide. The southern end of the transition region extended as a shallow, nearly horizontal layer which was traversed by the aircraft during an ascent. The formation of a horizontal layer with temperatures near 0°C is driven by the melting of precipitation in the warmer air. The melting-induced cooling amplifies the vertical gradient of the temperature on the warm side of the 0°C layer and effectively decouples the regions below and above the isothermal layer. Our observations indicate that this mechanism was not dominant in this case and that possibly other factors, such as ascending motions and horizontal advection, were acting to destroy the melting induced isothermal layer.

The observations obtained during the horizontal pass through the transition region showed a sharp horizontal gradient of temperature present at the cold edge of the transition region. The freezing of cloud droplets onto ice particles and the refreezing of semi-melted particles in the adjacent cold region would diabatically warm the cold air and would tighten the horizontal temperature gradient on the cold side of the transition region. A large variability in the FSSP spectra as a function of the location from the cold edge of the transition region was observed. Fairly "fresh" FSSP distributions with large number concentrations (up to 300 cm^{-3}) were present in the transition region, although "old" parcels with bimodal distributions were also observed. Some large precipitation particles were present within this region. There was a section, a few kilometers wide, adjacent to the cold sector in the transition region (at 80 kPa) in which there was a virtual absence of particles larger than 25 μm.

The trajectory calculations are somewhat consistent with the aircraft observations and imply that there may be a zone of reduced particle concentrations in the

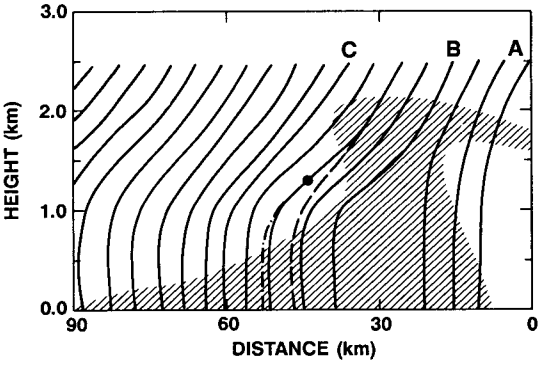

FIG. 11. Trajectories of particles having a mass equivalent to 1.5 mm diameter drop. The solid lines indicate trajectories determined by assuming that the atmosphere is saturated with respect to liquid water. The dashed line indicates one trajectory assuming that the vertical motion is zero. The dash-dot line indicates one trajectory which assumes saturation with respect to ice when below 0°C. The filled circle indicates the center of the updraft region with maximum value of 0.4 m s^{-1}. The transition region is shaded. *A*, *B*, and *C* refer to particles discussed in the text.

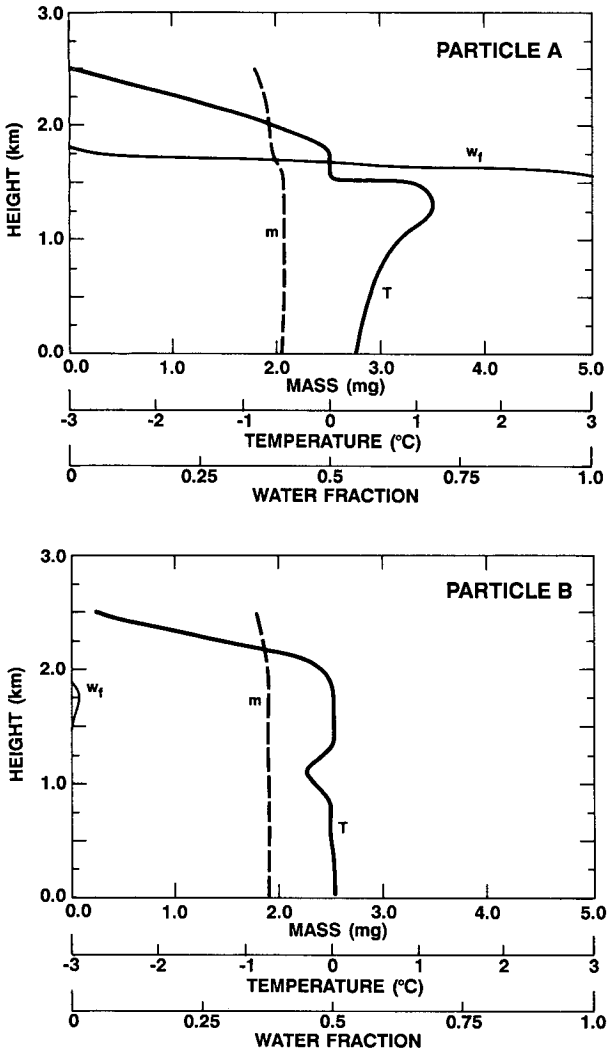

FIG. 12. The evolution of three of the 1.5 mm diameter equivalent drops shown in Fig. 11. The thick solid line corresponds to the particle temperature in °C (T), the dashed line corresponds to the particle mass in mg (m) and the thin solid line corresponds to the water fraction (w_f).

transition region. On the other hand, they do not predict the complete absence of large particles observed within the transition region. The observations also showed that large semi-melted particles were present at 86.5 kPa at temperatures below 0°C. This agrees with the fact that some of the calculated trajectories pass through the transition region and then into the colder air, resulting in partially melted particles.

b. *Conceptual model*

The analyzed thermodynamic and kinematic fields suggest a conceptual model for the circulation that resembles the synoptic conveyor belts, discussed by Carlson (1980), Browning and Monk (1982), and Stewart and Macpherson (1989), but on a much smaller scale. In this instance, the jet within the *cold conveyor belt* is located just north of the precipitation type transition region and the warm southerly air (*warm conveyor belt*) rises over the *cold conveyor belt*. As mentioned previously, the region studied was located close to the analyzed low pressure centers at the surface and aloft. Earlier high resolution studies have not investigated the regions near the low pressure centers. At least in this case, the temperature structure very close to the low pressure center was affected by microphysical processes.

A two-dimensional schematic highlighting some of the processes discussed is shown in Fig. 14. The transition region (shaded) corresponds to the boundary between the ascending, moist, southerly air with high cloud liquid water contents (*warm conveyor belt*, labeled WCB in Fig. 14) and the relatively cold easterly jet (*cold conveyor belt*, labeled CCB in Fig. 14). The thick solid line labeled 0 m s^{-1} represents the boundary between easterly and westerly flow. Melting occurs on the warm side of the transition region, where particles up to 9 mm in diameter are observed. Freezing of

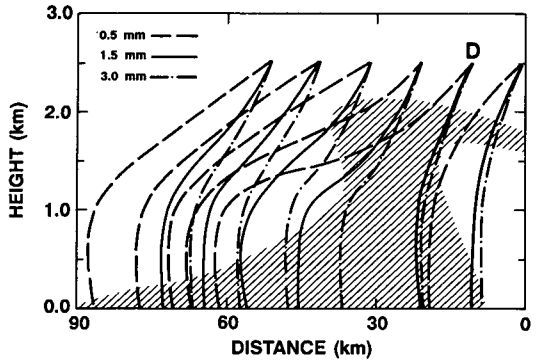

FIG. 13. Trajectories of particles having masses equivalent of 0.5, 1.5, and 3.0 mm diameter drops. The air is assumed to be saturated with respect to water. The transition region is shaded. *D* refers to the location of particles discussed in text.

droplets and semi-melted particles occurs on the cold side of the transition region. Immediately downwind of the transition region the air temperature dropped to −3°C. The largest ice crystals (aggregates of columns) were observed in this region at 80 kPa. There was evidence of riming in a large fraction of the ice particles, which is probably linked to the influx of air with high number concentration of cloud droplets. At lower levels, the northerly edge of the transition region coincided with a region of large horizontal wind shear and turbulence, adjacent to the maximum values of easterly winds (*cold conveyor belt*). Riming, aggregation and possibly ice multiplication were active near and above the transition region, where a weak westerly jet was present. Because of the environmental temperature and wind fields, the trajectories of particles near the transition region may lead to regions of enhanced as well as reduced concentrations at the surface and aloft. The detailed nature of the particles affects their trajectories and consequently their evolution and distribution.

It is reasonable to ask how valid is this two-dimensional schematic picture that we have just discussed. The observations obtained by the aircraft 40–50 km east of the cross section presented here (see Fig. 1), show the same kinematic patterns of cold and warm conveyor belts. The thermal structure also shows a transition region about 20 km wide at 86 kPa, but this region does not extend up to 79 kPa. The microphysical characteristics (cloud and precipitation particles) show the same overall pattern as in the cross section at 63°W. The main differences are that the number concentration of precipitation particles is about a factor 4 larger 40 km east of the cross section at 63°W and that it is not as obvious as before that some particles had par-

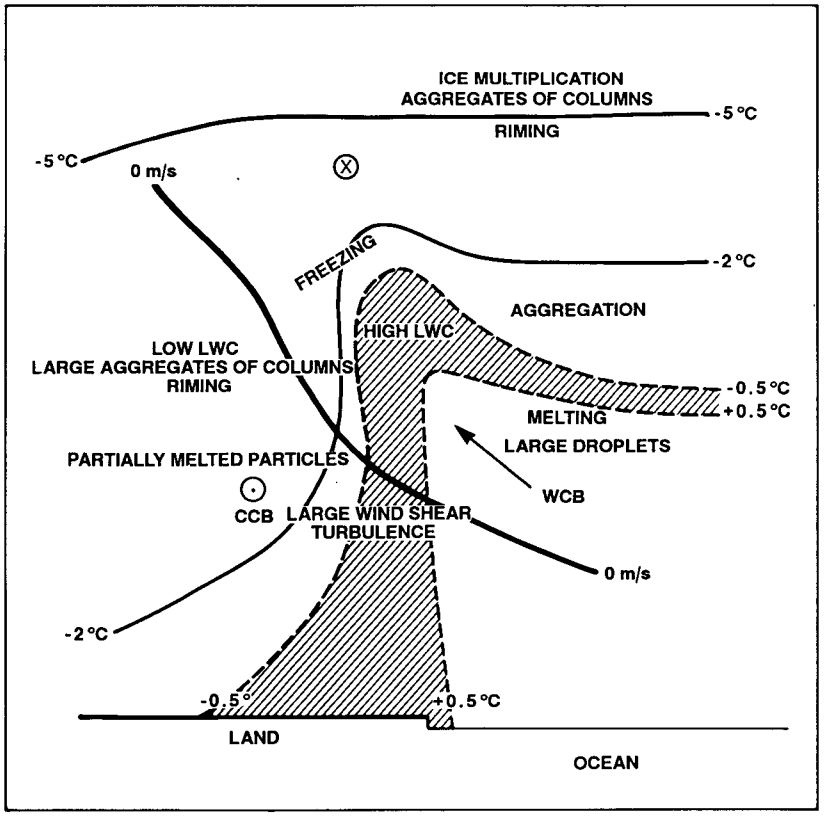

FIG. 14. Schematic figure showing conceptual model discussed in text.

tially melted and refrozen. Nevertheless, most of the characteristics and processes described in our conceptual model are present 40 km east, providing support for a two-dimensional assumption.

In summary, this article has illustrated with insitu information some of the many couplings between microphysical, thermodynamic, and dynamic features that occur in the region of winter storms associated with the transitions between precipitation types. Many of the processes described in this study are likely to occur in other cases with transition regions. However, it is certainly recognized that further studies are needed to verify this, and it would be particularly useful to examine transition regions not directly linked to a topographic feature.

Acknowledgments. This research was supported in part by the Federal Panel on Energy Research and Development (PERD). The authors are grateful to J. W. Strapp and A. Madej for their assistance in the processing of the aircraft data.

REFERENCES

Best, A. C., 1950: Empirical formulae for the terminal velocity of water drops falling through the atmosphere. *Quart. J. Roy. Meteor. Soc.*, **95,** 544–560.

Browning, K. A., and G. A. Monk, 1982: A simple model for the synoptic analysis of cold fronts. *Quart. J. Roy. Meteor. Soc.*, **108,** 435–452.

Carlson, T. N., 1980: Airflow through midlatitude cyclones and the comma cloud pattern. *Mon. Wea. Rev.*, **108,** 1498–1509.

Donaldson, N. R., and R. E. Stewart, 1991: Precipitation type characteristics in winter storms. Part I: Basic simulations. *J. Atmos. Sci., to be submitted.*

Gordon, G., and Marwitz, J. D., 1984: An airborne comparison of three PMS probes. *J. Atmos. Oceanic Technol.*, **1,** 22–27.

Hallett, J., and S. C. Mossop, 1974: Production of secondary ice particles during the riming process. *Nature,* **294,** 26–28.

Heymsfield, A. J., and J. L. Parrish, 1979: Techniques employed in the processing of particle size spectra and state parameter data obtained with the T-28 aircraft platform. NCAR Tech. Note NCAR/TN-137+1A, 78pp.

Hobbs, P. V., 1978: Organization and structure of clouds and precipitation on the mesoscale and microscale in cyclonic storms. *Rev. Geophy. Space Phys.*, **16,** 741–755.

Knight, D. J., and P. V. Hobbs, 1988: The mesoscale and microscale structure and organization of clouds and precipitation in midlatitude cyclones. XV: A numerical modeling study of frontogenesis and cold-frontal rainbands. *J. Atmos. Sci.*, **45,** 915–930.

Lin, C. A., and R. E. Stewart, 1986: Mesoscale circulation initiated by melting snow. *J. Geophys. Res.*, **91,** 13 299–13 302.

List, R., N. R. Donaldson and R.E. Stewart, 1987: Temporal evolution of drop spectra to collisional equilibrium in steady and pulsating rain. *J. Atmos. Sci.*, **44,** 362–372.

Matsuo, T., and Y. Sasyo, 1981: Melting of snowflakes below freezing level in the atmosphere. *J. Meteor. Soc. Japan,* **59,** 10–24.

Parsons, D. B., and P. V. Hobbs, 1983: The mesoscale and microscale structure and organization of clouds and precipitation in midlatitude cyclones. VII: Formation, development, interaction and dissipation of rainbands. *J. Atmos. Sci.*, **40,** 559–579.

Sanders, F., and L. Bosart, 1985: Mesoscale structure in the megalopolitan storm of 11–12 Feb. 1983. Part I: Frontogenetical forcing and symmetric instability. *J. Atmos. Sci.*, **42,** 1050–1061.

Stewart, R. E., and P. King, 1987a: Freezing precipitation in winter storms. *Mon. Wea. Rev.*, **115,** 1270–1279.

——, and ——, 1987b: Rain-snow boundaries over southern Ontario. *Mon. Wea. Rev.*, **115,** 1894–1907.

——, and L. M. Patenaude, 1988: Rain-snow boundaries and freezing precipitation in Canadian East Coast winter storms. *Atmos.-Ocean,* **26,** 377–398.

——, and S. R. Macpherson, 1989: Winter storm structure and melting-induced circulations. *Atmos.-Ocean,* **27,** 5–23.

——, J. D. Marwitz, J. C. Pace and R. E. Carbone, 1984: Characteristics through the melting layer of stratiform clouds. *J. Atmos. Sci.*, **41,** 3227–3237.

——, R. W. Shaw and G. A. Isaac, 1987: Canadian Atlantic Storms Program: The meteorological field project. *Bull. Amer. Meteor. Soc.*, **68,** 338–345.

——, C. A. Lin and S. R. Macpherson, 1990: The structure of a winter storm producing heavy precipitation over Nova Scotia. *Mon. Wea. Rev.*, **118,** 411–426.

Vardiman, L., 1978: The generation of secondary ice particles in clouds by crystal–crystal collisions. *J. Atmos. Sci.*, **35,** 2168–2180.

Willis, P. I., and A. J. Heymsfield, 1989: Structure of the melting layer in mesoscale convective system stratiform precipitation. *J. Atmos. Sci.*, **46,** 2008–2025.